Selective production of hydrogen for fuel cells via oxidative steam reforming of methanol over CuZnAl oxide catalysts: effect of substitution of zirconium and cerium on the catalytic performance

S. Velu[a,b,*] and K. Suzuki[a]

[a]Ceramics Research Institute, National Institute of Advanced Industrial Science and Technology (AIST), Nagoya-462 8510, Japan
[b]Present address: The Energy Institute, and the Department of Energy and Geo-Environment Engineering, The Pennsylvania State University, 209 Academic Projects Building, University Park, PA 16802, USA

H_2 fuel, for fuel cells, is traditionally produced from methanol by the endothermic steam reforming of methanol (SRM). Partial oxidation of methanol (POM), which is highly exothermic, has also been suggested as a route to extract H_2 from methanol. In both these reactions a considerable amount of CO is produced as a byproduct, which is a poison to the Pt anode of the fuel cell. A combined steam reforming and partial oxidation of methanol, which has been termed "oxidative steam reforming of methanol" (OSRM), reported recently is considered to be more efficient and convenient for the selective production of H_2 at a relatively low temperature. The catalysts used in the OSRM reaction were CuZnAl mixed oxides derived from hydroxycarbonate precursors containing hydrotalcite (HT)-like layered double hydroxides (LDHs)/aurichalcite phases. Substitution of Zr for Al in the CuZnAl oxide system was found to improve the catalytic performance. In the present study, the role of added Zr was investigated in detail by employing spectroscopic methods such as X-ray diffraction (XRD), temperature-programmed reduction (TPR), electron paramagnetic resonance (EPR) spectroscopy, X-ray photoelectron spectroscopy (XPS) and X-ray induced Auger electron spectroscopy (AES). The detailed spectroscopic studies revealed that substitution of Zr for Al improved the reducibility and dispersion of copper species due to the operation of a synergistic interaction between copper and zirconium as a consequence of the formation of a "Cu^{2+}–O–Zr^{4+}–O–" solid solution. The higher catalytic performance of CuZn-based catalysts containing Zr in the OSRM reaction was attributed to the ease of reducibility and enhanced dispersion of copper particles on the support. The substitution of Ce in the CuZnAl system, on the other hand, did not alter the catalytic performance greatly.

KEY WORDS: H_2 production; steam reforming of methanol; partial oxidation of methanol; autothermal reforming of methanol; CuZn-based catalysts; layered double hydroxides

1. Introduction

Fuel cells have emerged recently as the most promising low-emission power generation system for vehicles. They are two to three times more efficient than internal combustion engines in terms of converting fuel to power and hence may eventually replace internal combustion engines as a clean, highly efficient source of power for all types of highway vehicles. The primary fuel for fuel cells is hydrogen (H_2), which can be extracted from natural gas, coal-gas, methanol, etc. Among them, methanol is considered to be an ideal fuel for generating H_2 onboard a vehicle because it is a liquid and easy to transport. Furthermore, it is one of the largest commodity chemicals and can be conveniently synthesized from natural gas, biomass or coal [1,2].

Hydrogen can be extracted from methanol according to three different processes: decomposition of methanol (DCM; equation (1)), partial oxidation of methanol (POM, equation (2)) and steam reforming of methanol (SRM, equation (3)) [2–5]:

$$\mathrm{CH_3OH}(\ell) \Leftrightarrow 2\mathrm{H_2(g)} + \mathrm{CO(g)};\ \Delta H^{\circ}_{298} = +128.1\,\mathrm{kJ\,mol^{-1}},\ \Delta G^{\circ}_{298} = +29.0\,\mathrm{kJ\,mol^{-1}} \quad (1)$$

$$\mathrm{CH_3OH}(\ell) + 1/2\mathrm{O_2(g)} \Leftrightarrow 2\mathrm{H_2(g)} + \mathrm{CO_2(g)};\ \Delta H^{\circ}_{298} = -154.9\,\mathrm{kJ\,mol^{-1}},\ \Delta G^{\circ}_{298} = -228.2\,\mathrm{kJ\,mol^{-1}} \quad (2)$$

$$\mathrm{CH_3OH}(\ell) + \mathrm{H_2O}(\ell) \Leftrightarrow 3\mathrm{H_2(g)} + \mathrm{CO_2(g)};\ \Delta H^{\circ}_{298} = +130.9\,\mathrm{kJ\,mol^{-1}},\ \Delta G^{\circ}_{298} = +8.9\,\mathrm{kJ\,mol^{-1}}. \quad (3)$$

While the DCM and SRM reactions are endothermic, the POM reaction is exothermic. The decomposition of methanol to CO and H_2 has been studied extensively by

* To whom correspondence should be addressed.
E-mail: vxs23@psu.edu

1022-5528/03/0400–0235/0

many researchers [2–7], because the syngas obtained from methanol is up to 60% more efficient than gasoline and up to 34% better than undecomposed methanol itself in terms of converting fuel to power. In addition, the endothermicity of the reaction is taken as an advantage as a heat recovery system in factories such as power plants and in iron manufacture. On the other hand, for the purpose of fuel cells in mobile applications, the SRM reaction is considered to be the most suitable, because the reaction produces stoichiometrically more H_2 (3 mol of H_2 from 1 mol of methanol) than is actually available in methanol alone on account of the participation of water in the overall process. Moreover, the byproduct is CO_2 rather than CO, the latter being a poison to the Pt anode of the fuel cells. Fierro and co-workers [4] have reported that, because of the exothermicity, the POM reaction is more energy efficient compared with the SRM reaction and could be employed for H_2 generation onboard a vehicle. However, the POM reaction produces stoichiometrically only 2 mol of H_2 from 1 mol of methanol. The authors of the present paper have recently demonstrated [8–11] that a combined steam reforming and partial oxidation of methanol referred to as the "oxidative steam reforming of methanol" (OSRM, equation (4)) reaction over CuZnAl(Zr) oxide catalysts is the most convenient way for onboard H_2 generation for fuel cells:

$$CH_3OH(\ell) + [1-(2\delta)]H_2O(\ell) + \delta O_2(g) \Leftrightarrow [3-(2\delta)]H_2(g) + CO_2(g) \quad (4)$$

If $\delta = 0.25$, $\Delta H^{\circ}_{298} = -12.0\,\mathrm{kJ\,mol^{-1}}$, $\Delta G^{\circ}_{298} = -109.6\ \mathrm{kJ\,mol^{-1}}$.

In the OSRM reaction, a mixture of methanol, water and air is passed through the catalyst bed. The ratio of these three reactants can be adjusted in such a way that the overall reaction is either thermally neutral or moderately exothermic (see equation (4)). Some of the advantages of the OSRM reaction are the following. (1) The reaction can be operated at lower temperature than that of the SRM reaction. (2) Since the heat necessary for the endothermic SRM reaction is supplied *in situ* by the exothermic POM reaction, an external heat supply can be avoided. (3) Easy start-up of the fuel processor. (4) The mild exothermicity of the reaction avoids hot-spot operation, which usually accompanies the POM reaction. (5) The reaction produces H_2 with very low outlet CO levels compared to that obtained in the SRM reaction. (6) Under optimized operating conditions the reaction produces close to 3 mol of H_2 from 1 mol of methanol. (7) Owing to the above reasons, the overall cost of the fuel processor unit can be minimized.

In earlier investigations [8,9,11] using CuZnAl(Zr) oxide catalysts, it was noticed that the substitution of Zr improves the catalytic performance in terms of methanol conversion and H_2 production rate. However, the role of Zr in these catalytic systems is not well understood, although bifunctional roles of Cu and ZrO_2 in the similar Cu/ZrO_2-supported catalysts have been suggested in the methanol synthesis as well as in the methanol decomposition reactions [12]. In the process of development of catalysts for the OSRM reaction, we have also synthesized CuZn-based catalysts containing Ce^{4+}, because cerium oxide in three-way catalysts is known to promote the water-gas shift (WGS) and CO oxidation reactions [13].

The objective of the present study is to investigate the effect of incorporation of Zr and Ce in CuZnAl(Zr) oxide catalysts on the catalytic performance in the OSRM reaction and to correlate the catalytic activity with the physicochemical properties of the catalysts, as investigated using spectroscopic techniques such as XRD, TPR, EPR, XPS and AES.

2. Experimental

2.1. Catalyst preparation

The precursors of CuZn-based oxide catalysts were prepared by the method of coprecipitation at a constant pH (≈10) [14]. An aqueous solution "A" containing a mixture of metal salts ($Cu(NO_3)_2$, $Zn(NO_3)_2$, $Al(NO_3)_3$, $ZrOCl_2$, $Ce(NH_4)_2(NO_3)_6$) in the desired proportion and solution "B" containing a mixture of NaOH and Na_2CO_3 were added dropwise (60 cm^3/h) at room temperature with vigorous stirring. The resulting gel was aged at 65 °C for 30 min. The precipitate was filtered and washed with excess distilled water until the pH of the filtrate was equal to the pH of the distilled water. Calcination of the precursors in a muffle furnace at 450 °C for 5 h yielded CuZn-based mixed oxide catalysts.

2.2. Catalyst characterization and activity measurements

Detailed procedures for the chemical analysis, X-ray diffraction (XRD), temperature-programmed reduction (TPR) and electron paramagnetic resonance (EPR) spectroscopy are described elsewhere [9,10]. The method for the measurement of BET surface area, pore volume (V_p) and pore radii (R_p), and the copper metal surface area by CO chemisorption were performed as reported already [11,15].

The core-level X-ray photoelectron (XP) spectra and the X-ray induced Auger electron (AE) spectra were acquired using a VG Microtech Multilab ESCA 3000 spectrometer. All measurements were made at room temperature using a non-monochromatized MgKα X-ray source ($h\nu = 1253.6$ eV) on powder samples. The base pressure in the analysis chamber was maintained at 3–6 $\times 10^{-10}$ torr. The energy resolution of the spectrometer was set at 0.8 eV with MgKα radiation at a pass

energy of 20 eV. Binding energy (BE) was calibrated with respect to the Au $4f_{7/2}$ core level at 83.9 eV. The BE of adventitious carbon (284.9 eV) was utilized for charge correction. The error in all the BE values reported in the present study is within 0.1 eV.

The OSRM reaction was performed in a conventional fixed-bed glass flow reactor (4 mm i.d.) using 100 mg of the catalyst (particle size 0.30–0.355 mm) in the temperature range 180–290 °C at atmospheric pressure. The experimental procedure for catalytic activity measurements is reported in more detail elsewhere [9–11].

3. Results

3.1. Effect of Zr substitution on catalytic activity and physicochemical properties

In earlier investigations [8,9] on the OSRM reaction over a series of CuZnAl oxide catalysts derived from LDH precursors it was observed that, among the catalysts, CuZnZr-1, with Cu : Zn : Al = 37.6:50.7:11.7 wt% (Cu : Zn : Al atomic ratio = 0.59:0.78:0.43), was the most active. In order to investigate the effect of substitution of Zr, the authors performed the OSRM reaction over two more samples containing 14.3 and 27.2 wt% Zr (CuZnZr-2, Cu:Zn:Al:Zr atomic ratio = 0.57 : 0.69 : 0.19 : 0.15; and CuZnZr-3, Cu:Zn:Al:Zr atomic ratio = 0.51 : 0.62 : 0.00 : 0.30, respectively). Figure 1 compares the effect of temperature on the catalytic performance in the OSRM reaction over these three catalysts. It can be clearly seen that substitution of Zr for Al further improves the catalytic performance in terms of both methanol conversion and H_2 production rate. The catalyst CuZnZr-3, containing Zr without Al, exhibits the highest methanol conversion and H_2 production rate. Although the CO selectivity is slightly higher over the same catalyst it remains considerably low (carbon selectivity up to about 1 mol%) in the temperature range studied.

In order to understand the role of Zr in these catalytic systems, the physicochemical properties of the catalysts have been investigated by means of TPR, EPR and XPS. The TPR profiles of the catalysts shown in figure 2 indicate that the maximum rate of H_2 consumption gradually shifts towards lower temperature with increasing Zr content. The CuZnZr-3 sample without Al exhibits the lowest onset temperature of around 160 °C. The first peak is centered at around 184 °C and the reduction completes itself around 240 °C. These results reveal that a decrease in Al content improves the copper reducibility. Alternatively, substitution of Zr for Al enhances the copper reducibility.

The EPR spectra of the CuZnZr-1, CuZnZr-2 and CuZnZr-3 catalysts are compared in figure 3. In all instances the spectra show the presence of two kinds of signals: signal A (2600–3200 G) exhibiting a resolved hyperfine pattern of four peaks, and signal B (around

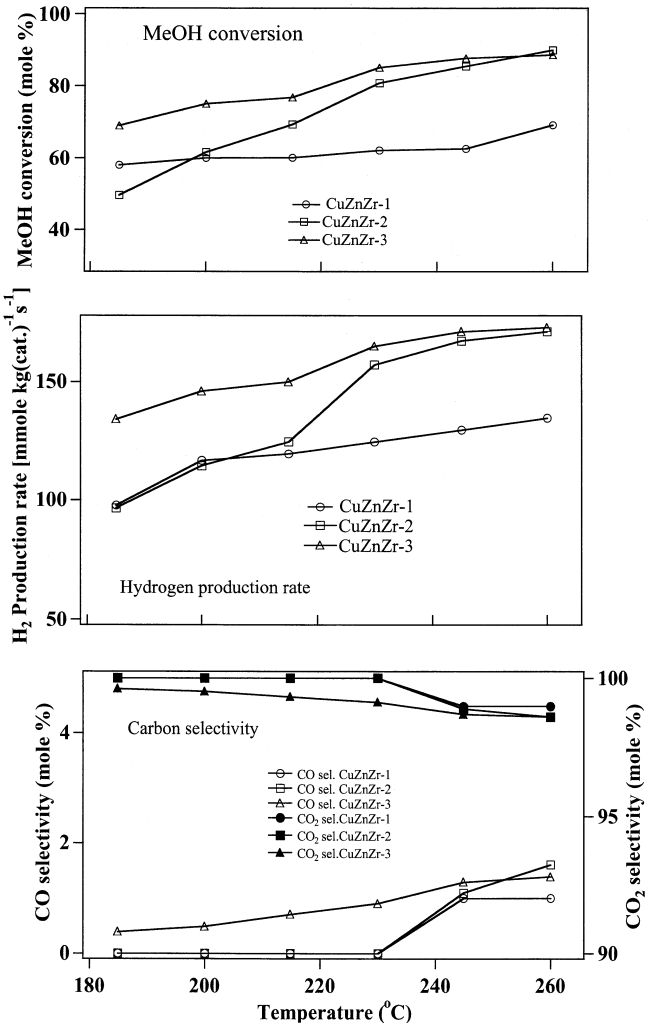

Figure 1. Effect of temperature on catalytic performance in the oxidative steam reforming of methanol over CuZnAl(Zr) oxide catalysts. Reaction conditions: catalyst weight = 100 mg; $H_2O/CH_3OH = 1.3$; liquid flow rate of feed = 2.5 cm^3/h; O_2/CH_3OH = 0.25; flow rate of Ar = 43 cm^3/min.

3300 G) without hyperfine structure. Both signals A and B are typical of Cu^{2+} ions. Signal B exhibiting unresolved hyperfine splitting could be attributed to the Cu^{2+} species interacting with each other and generally referred to as "clustered Cu^{2+} ions". On the other hand, signal A with a resolved hyperfine pattern could be interpreted as arising from distorted octahedrally coordinated Cu^{2+} ions [13,16–18]. The four-line hyperfine splitting is typical of isolated Cu^{2+} ions in an axial environment and shows a hyperfine structure better resolved in the $g_{\|}$ component. A closer inspection of the spectra indicates that the hyperfine structure of the $g_{\|}$ components is due to the superimposition of two sets of four hyperfine lines. The EPR parameters of the paramagnetic components employed in the simulation of experimental spectra are for component 1: $g_{\|} = 2.323$, $g_{\perp} = 2.065$, $A_{\|} = 153$ G and $A_{\perp} = 35$ G; for component 2: $g_{\|} = 2.343$, $g_{\perp} = 2.070$, $A_{\|} = 144$ G and $A_{\perp} = 15$ G. The presence of two sets of EPR signals

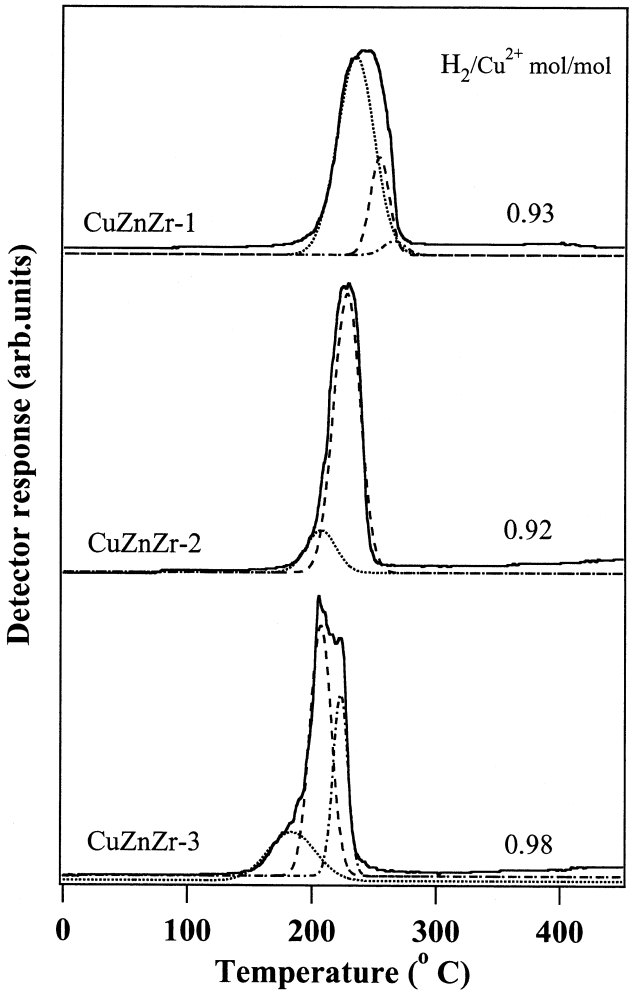

Figure 2. TPR profiles of CuZnAl(Zr) oxide catalysts. Solid lines are experimental curves and dotted/broken lines are deconvoluted curves.

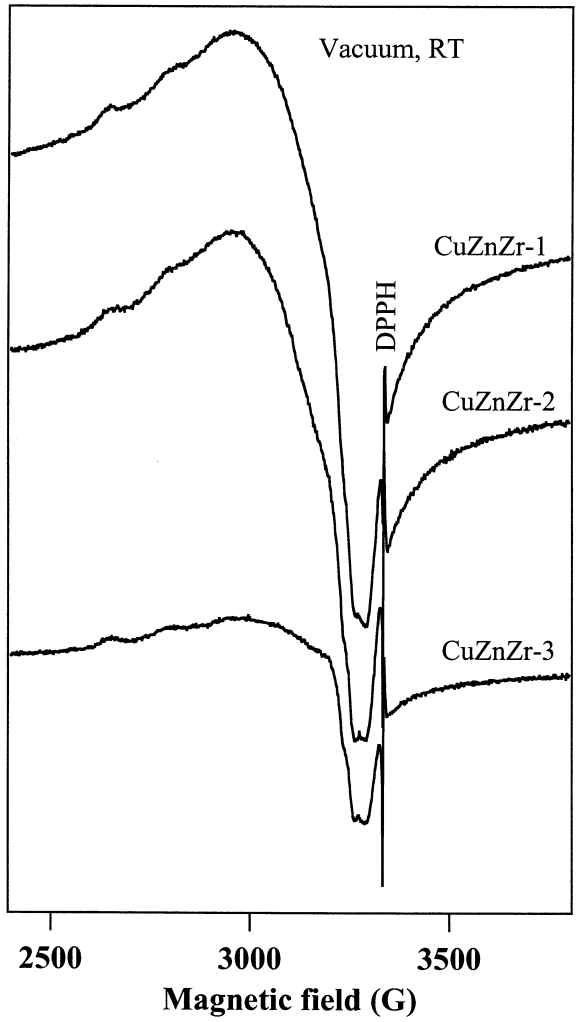

Figure 3. EPR spectra of CuZnAl(Zr) oxide catalysts recorded under vacuum at room temperature (≈ 298 K).

(component 1 and component 2) reveals that there are two slightly different kinds of copper ions present in the system. The component 2 signal, which is characterized by higher $g_{\|}$ and lower $A_{\|}$ values, corresponds to Cu^{2+} species undergoing a more axial interaction than that of component 1 species [18].

It is also noticed that, in all cases, the EPR signals did not recover the baseline, suggesting a large contribution of a broad component. Another interesting feature noticed from the EPR spectra is that the EPR signal intensity (amplitude) is strongly influenced by the chemical compositions. For instance, the signal amplitude around 3000 G is reduced to a great extent and the overall intensity is reduced by about three-fold when Zr replaces Al in the sample. It should be mentioned that the signal intensity of EPR is proportional to the spin concentration of the isolated Cu^{2+} ion [19]. Hence, the reduction in the EPR signal intensity upon substitution of Zr for Al can be attributed to the reduction of the amount of isolated Cu^{2+} ions. So, the result implies that in the Zr-containing catalysts a large amount of CuO-like clusters are present. Similar results were also observed for Cu–Zn mixed oxide systems without Al as well as for Cu supported on Y-stabilized ZrO_2 catalyst [18,19].

XPS studies have been undertaken in order to further understand how the chemical state and electronic properties at the surface of the catalysts are modified upon Zr substitution. Figure 4 displays Cu $2p$ core-level XPS spectra of the CuZnAl oxide catalyst without Zr (CuZnZr-1), the catalyst containing both Zr and Al (CuZnZr-2) and the catalyst containing Zr without Al (CuZnZr-3). It can be seen that these samples exhibit Cu $2p_{3/2}$ and Cu $2p_{1/2}$ main peaks in the binding energy (BE) ranges 933–934 and 953–954 eV, respectively, with a spin–orbit coupling energy gap of 20 eV. The BEs of Al-containing CuZnZr-1 and CuZnZr-2 samples are close to each other while for CuZnZr-3 containing Zr without Al it is 933.4 eV (see table 3). It can also be noticed that both Cu $2p_{3/2}$ as well as Cu $2p_{1/2}$ peaks is accompanied by intense satellite features at 942 and 962 eV for all samples. The intensity ratio between the satellite and the Cu $2p_{3/2}$

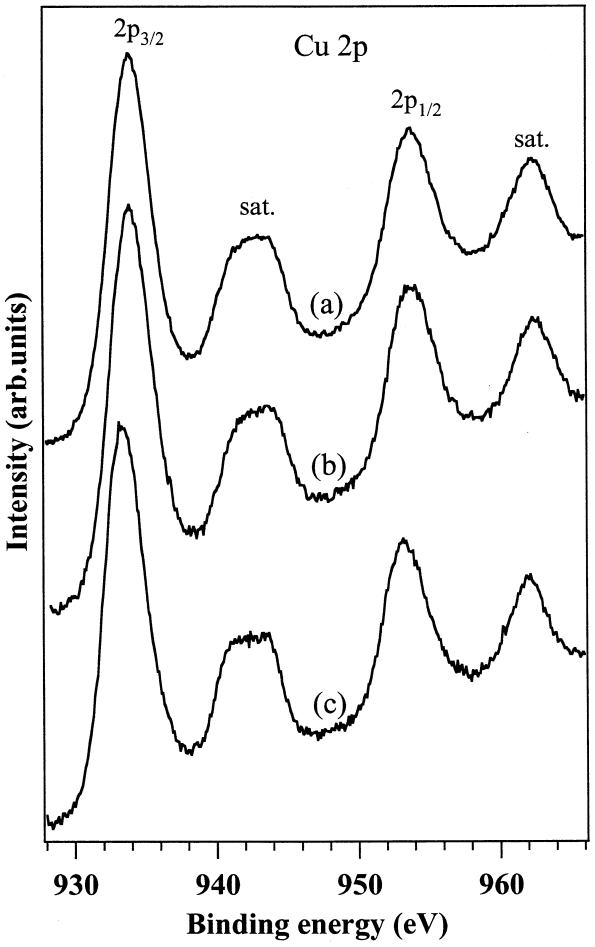

Figure 4. Cu 2*p* core-level X-ray photoelectron spectra of CuZnAl(Zr) oxide catalysts: (a) CuZnZr-1, (b) CuZnZr-2, (c) CuZnZr-3.

main band (I_S/I_M = 0.40–0.46) and the full-width at half maximum (FWHM = 3.2 ± 0.1 eV) are almost the same for all the catalysts.

The X-ray induced Auger electron spectra (AES) of these samples are presented in figure 5 in the kinetic energy (KE) region between 904 and 930 eV. The XP spectrum of pure ZrO_2 reference sample in the Zr 3*p* region is also included. The position of the peaks due to the Cu $L_3M_{45}M_{45}$ (hereafter referred to as Cu LMM) transition of Cu^{2+} in the KE range 913–919 eV can be clearly distinguished from Zr $3p_{5/2}$ at 920.8 eV in the Zr-containing samples (the data are included in table 3). As observed in the core level, the position of the Cu Auger peak also shifts with respect to the chemical composition. The modified Auger parameter (α') has been used to determine the chemical state of copper in these samples. The parameter α' is defined as:

$$\alpha' = h\nu + (\text{KE Cu LMM} - \text{KE Cu}2p_{3/2}) \qquad (5)$$

where $h\nu$ is the energy of the incident photon (1253.6 eV) and KE Cu LMM and KE Cu $2p_{3/2}$ are the kinetic energies of the corresponding Auger electron and core-level photoelectron, respectively. The α' values determined using equation (5) are included in table 3 together with data for some of the reference samples containing Cu^{2+} [20–22]. Similarly to that observed in the Cu 2*p* core level, the Auger KE and α' of CuZnZr-1 and CuZnZr-2 are similar (around 917 eV and 1850.8 ± 0.1 eV) while for CuZnZr-3 they are 918.0 and 1851.4 eV, respectively. The observed difference in the BE and α' values between these samples clearly points to a different electron density on the copper atoms.

Zn $2p_{3/2}$ core-level XP spectra of all the samples (data not shown) exhibited an intense peak at 1021.9 ± 0.2 eV with a FWHM value of about 2.2 ± 0.1 eV, very close to the BE (1021.3–1022.0 eV) and FWHM (2.0 eV) of ZnO reference [20]. This indicated that the chemical environment of Zn was not affected due to the change in the chemical composition.

Zr 3*d* core-level XP spectra of CuZnZr-2 containing both Al and Zr and CuZnZr-3 without Al are shown in figure 6 together with the spectrum of pure ZrO_2. It can be seen that the pure ZrO_2 exhibits a spin–orbit doublet of the 3*d* core level into $3d_{5/2}$ (182.1 eV) and $3d_{3/2}$ (184.5 eV) levels with an energy gap of 2.4 eV between them and a relative intensity ratio ($I_{3d5/2}/I_{3d3/2}$) of 1.6. These values are in excellent agreement with those reported in the literature for pure ZrO_2 [23]. The CuZnZr-2 and CuZnZr-3 samples also exhibit a similar doublet in the same BE region, indicating the existence of ZrO_2-like species. However, compared to ZrO_2, the catalyst samples exhibit broad bands and also the depth of the valley between the spin–orbit doublet is less. Deconvolution of the original spectra produces peaks

Table 1
Chemical compositions and XRD phases of CuZnAl(Zr) oxide catalyst precursors

Catalyst	Metal composition[a] (wt%)				(Cu + Zn)/(Al + Zr) atomic ratio[a]	XRD phase obtained[b]
	Cu	Zn	Al	Zr		
CuZnZr-1	37.6	50.7	11.7	0.0	3.31	LDH + AH + AC
CuZnZr-2	35.9	44.7	5.1	14.3	3.59	AC + LDH + AH
CuZnZr-3	32.3	40.5	0.0	27.2	3.79	AC

[a]Chemical analyses results obtained from XRF spectroscopy.
[b]LDH = layered double hydroxide ($((CuZn)_6Al_2(OH)_{16}CO_3.4H_2O$), JCPDS file 38–487; AH = $Al(OH)_3$ (bayerite), JCPDS file 20–11; AC = aurichalcite ($((Zn,Cu)_5(CO_3)_2(OH)_6$), JCPDS file 7–743.

Table 2
Textural properties of CuZnAl(Zr) oxide catalysts

Catalyst	N_2 adsorption–desorption measurement		CO chemisorption experiments		S_{cu} ($m^2 g^{-1}$)[a]	t_{Cu} (Å)[b]	D_{cu} (%)[c]
	BET surface area ($m^2 g^{-1}$)	Pore volume ($cm^3 g^{-1}$)	Pore radius (Å)	Amount chemisorbed ($\mu mol\, g^{-1}$)			
CuZnZr-1	108	0.428	80	831.7	34.4	112	14.1
CuZnZr-2	65	0.172	40	989.3	41.0	90	17.5
CuZnZr-3	59	0.099	20	1058.1	43.8	76	20.8

Note: These parameters were derived from CO chemisorption experiments [11,15].
[a] S_{Cu} = copper metal surface areas.
[b] t_{Cu} = particle sizes of metallic copper.
[c] D_{cu} = copper metal dispersion.

attributed to the existence of at least two kinds of Zr^{4+} species, namely species I at low BE and species II at high BE, differing in their chemical environments. A spin–orbit energy gap of 2.4 eV and an intensity ratio close to 60:40 for $3d_{5/2} : 3d_{3/2}$ have been imposed in this deconvolution. The peak positions and their contributions extracted from the deconvolution are summarized in table 4. The depth of the valley between the spin–orbit doublet is less in the case of CuZnZr-2, indicating a larger contribution of higher BE Zr species (species II). The concentration of species I increases at the expense of species II in CuZnZr-3. It can be noticed that the BE of species II is very close to that of ZrO_2 and hence they are assigned to ZrO_2-like species. The presence of an additional lower BE Zr species (species I) in these catalysts is interesting and suggests the formation, at the surface, of zirconium sites having relatively high electron density. The presence of a similar lower BE Zr^{4+} species has been observed in $Fe(NO_3)_3$-impregnated ZrO_2 and this indicated the involvement of a redox mechanism in iron-promoted zirconia catalysts [23].

Valence bands are those occupied by electrons of low BE (below 15 eV), which are essentially involved in the bonding orbitals. The measurement of spectra in this region is very useful to understand the electronic structure of materials. The main valence band (VB) below 7 eV is shown in figure 7. It can be seen that the VB spectra of the catalysts exhibit broad features around 4 eV. In this region, there could be contributions from valence orbitals of all the relevant elements (Cu, Al, Zr and O). However, owing to the high ionic character of Al^{3+} and Zr^{4+}, they do not contribute to the VB and their first lowest occupied core levels of Al 2*p* and Zr 4*p* appear around 74 and 30 eV, respectively. At the incident X-ray energy (1253.6 eV) employed in the present experiments, the photoionization cross-sections of O 2*p* and Cu 3*d* are 0.0005 and 0.021 Mb, respectively, and this factor influences the spectral intensity [24]. The above data clearly suggest that the Cu 3*d* have a larger contribution than O 2*p* to the VB, and the broad band around 4 eV can therefore be ascribed to the Cu 3*d* bands. It should be noted that in the present catalyst systems the highest occupied band consists mainly of Cu 3*d* character and hence the physicochemical properties of these materials depend on the chemical states of copper species. It is interesting to note that the BE of Cu 3*d* bands for CuZnZr-1 and CuZnZr-2 is higher (4.4 ± 0.1 eV) compared to that of CuZnZr-3 (around 3.7 eV). These results are in accord with those observed in the core-level XP spectra and suggest a significant modification in the electronic structure of copper species at the catalyst surface with respect to the chemical composition.

Another interesting observation noticed in the VB spectra of these catalysts is the appearance of a shoulder

Table 3
XPS and AES parameters of Cu $2p_{3/2}$ from CuZnAl(Zr) oxide catalysts and some reference compounds

Catalyst	BE of Cu $2p_{3/2}$ (eV)	FWHM (eV)	I_S/I_M	KE of Cu $L_3M_{45}M_{45}$ (eV)	α' (ev)
CuZnZr-1	933.8	3.3	0.46	916.9	1850.7
CuZnZr-2	933.9	3.3	0.40	917.0	1850.9
CuZnZr-3	933.4	3.1	0.44	918.0	1851.4
CuZnAl-HT [20]	934.6	3.8	–	916.0	1850.6
Malachite [20]	934.6	3.3	–	916.8	1851.4
CuO [21]	933.8	3.6	0.55	917.6	1851.4
$CuAl_2O_4$ [22]	935.0	–	–	916.5	1851.5

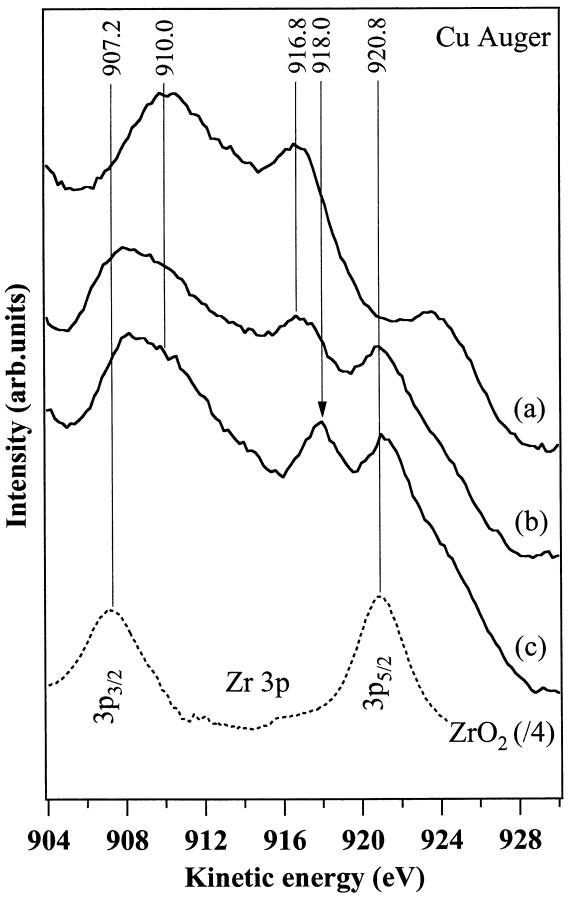

Figure 5. X-ray induced Auger electron spectra of CuZnAl(Zr) oxide catalysts: (a) CuZnZr-1, (b) CuZnZr-2, (c) CuZnZr-3. The core-level XP spectrum of ZrO_2 in the 3*p* region is also included.

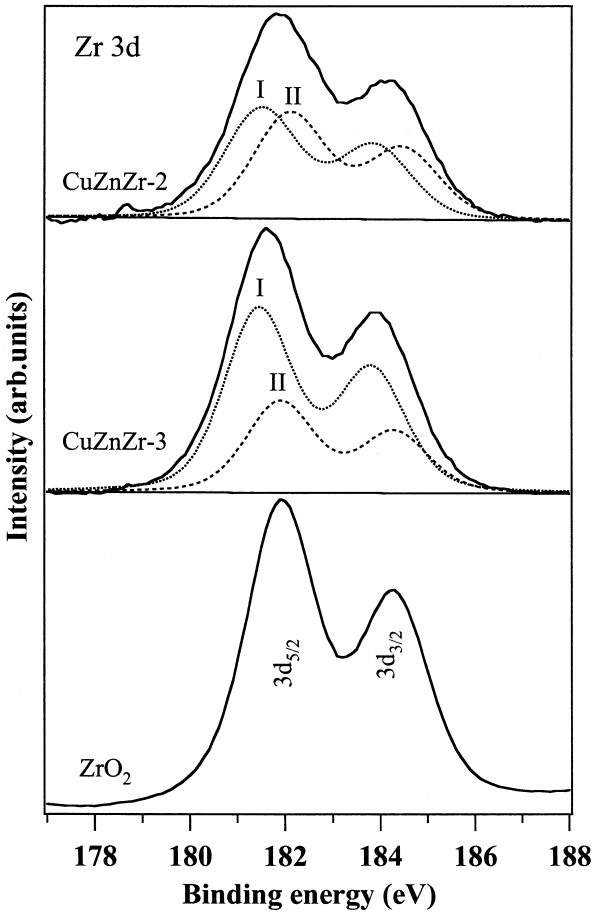

Figure 6. Zr 3*d* core-level X-ray photoelectron spectra of CuZnZr-2 and CuZnZr-3 catalysts. The Zr 3*d* core levels are deconvoluted to show the presence of two species. Species I occurs at low BE and species II at high BE. The spectrum of pure ZrO_2 is included for comparison.

around 2.3 eV, especially for CuZnZr-3. A similar shoulder, albeit with low intensity, can be noticed for CuZnZr-2 while it is very weak or absent for CuZnZr-1. This shoulder appears apparently due to splitting of the main VB feature around 3.7 eV and can be assigned to the anti-bonding orbitals of Cu 3*d* level [25,26].

3.2. *Effect of Ce substitution on the structural properties and catalytic activity*

Cerium oxide (CeO_2) is used widely as a promoter in the "three-way catalysts" for automobile exhaust gas treatment, in which the active component is formed mainly by Pt group metals dispersed on CeO_2/Al_2O_3 supports. CeO_2 stabilizes the Al_2O_3 support and maintains a high surface area, prevents the precious metals from sintering and thus stabilizes their dispersed state. It is also known to promote CO oxidation and WGS reactions [13,27,28]. The high activity of ceria in various redox reactions has generally been attributed to its reducibility and high oxygen storage capacity (OSC), and formation of defects, such as oxygen vacancies. Ce–Zr–O solid solutions have been extensively studied recently because of their unusual reduction behavior and high OSC [29]. Recent reports have shown that the oxidation activity of ceria can be much enhanced not only by the Pt metals but also by transition metals in general [30]. Thus, for systems containing both copper and ceria, the formation of intimate copper–ceria contacts is thought to be the crucial factor for the remarkably high activities exhibited for methanol synthesis or for the CO oxidation reaction [13,31].

Taking into account the enhanced catalytic activities observed in the CO oxidation and WGS reactions, the authors thought that the incorporation of Ce in the CuZnZr oxide catalysts would further improve the

Table 4
Zr 3*d* XPS parameters of CuZnAl(Zr) oxide catalysts and pure ZrO_2 reference sample

Catalyst	BE of Zr $3d_{5/2}$ core level (eV)	
	Species I (% intensity)	Species II (% intensity)
CuZnZr-2	181.5 (51.1)	182.1 (48.9)
CuZnZr-3	181.4 (66.8)	181.9 (33.2)
ZrO_2	None	181.9 (100)

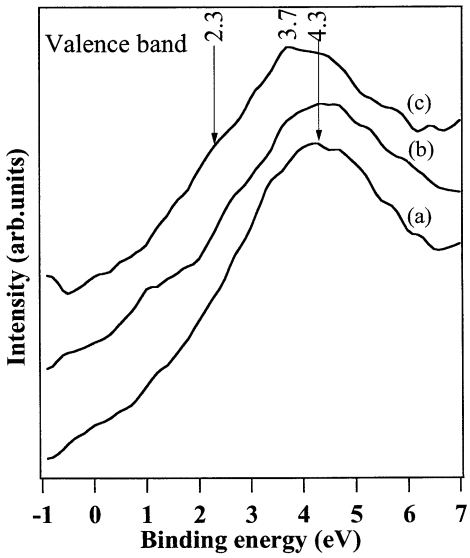

Figure 7. Valence band X-ray photoelectron spectra of CuZnAl(Zr) oxide catalysts: (a) CuZnZr-1, (b) CuZnZr-2, (c) CuZnZr-3.

catalytic performance in the OSRM reaction and reduce the outlet CO level. Thus, a series of CuZnZrCe oxide catalysts with various Cu:Zn:Zr:Ce ratios were synthesized by the coprecipitation method (table 5) and the catalytic activity was tested in the OSRM reaction.

The catalytic data summarized in table 6 indicate that, although there is only a minor improvement in the methanol conversion (about 7 mol%) and H_2 production rate (about 10 mmol/kg(catalyst)/s) over the CuZnCe-3 catalyst containing 20 wt% Ce, the outlet CO level and the RH_2/RMeOH ratio remain almost unaffected (compare the results of CuZnZr-3 and CuZnCe-3). In fact, the methanol conversion decreases with further increase in Ce content beyond 20 wt%. Since ceric ammonium nitrate (CAN) salt has been used as a precursor of Ce, it has been assumed that some of the Cu would have been leached out by the formation of a soluble copper amine complex during the precipitation of catalyst precursors containing 40 and 60 wt% copper. Hence, catalysts were also synthesized using Ce(IV)SO_4

Table 5
Chemical composition and XRD phases of CuZnZrCe oxide catalysts and their precursors

Catalyst	Cu:Zn:Zr:Ce (wt%)	XRD phase obtained	
		Uncalcined samples	Calcined samples (450 °C/5 h)
CuZnCe-1	35.5:39.5:15.0:10.0	Aurichalcite + hydrozincite	CuO + ZnO
CuZnCe-2	35.5:49.5:0.0:15.0	Aurichalcite + hydrozincite	CuO + ZnO + CeO_2
CuZnCe-3	35.5:29.5:15.0:20.0	Aurichalcite + hydrozincite	CuO + ZnO + CeO_2
CuZnCe-4	35.5:9.5:15.0:40.0	Aurichalcite + CeO_2	CuO + ZnO + CeO_2
CuZnCe-5	35.5:0.0:4.5:60.0	Aurichalcite + CeO_2	CuO + CeO_2
CuZnCe-6[a]	35.5:29.5:15.0:20.0	Aurichalcite + hydrozincite	CuO + ZnO + CeO_2
CuZnCe-7[b]	35.5:29.5:15.0:20.0	Aurichalcite + hydrozincite	CuO + ZnO + CeO_2
CuZnCe-8[a]	35.5:0.0:4.5:60.0	Aurichalcite + CeO_2	CuO + CeO_2

Note: Aurichacite = $(Zn, Cu)_5(CO_3)_2(OH)_6$ (JCPDS file No. 7–743); hydrozincite = $Zn_5(CO_3)_2(OH)_6$ (JCPDS file No. 19–1458).
[a]Ce(IV)SO_4 salt was used as precursor.
[b] Ce(III)NO_3 salt was used as precursor.

Table 6
Catalytic results of the oxidative steam reforming of methanol over CuZnZrCe oxide catalysts

Catalyst	MeOH conversion (mol%)	Rate of product formation (mmol kg(catalyst)$^{-1}$ s^{-1})			Outlet CO level (mol%)[a]	RH_2/RMeOH[b]
		H_2	CO	CO_2		
CuZnZr-3	71.7	108.0	0.22	37.8	0.083	2.84
CuZnCe-1	66.8	101.4	0.23	35.2	0.090	2.86
CuZnCe-2	71.8	110.1	0.37	37.7	0.130	2.89
CuZnCe-3	78.5	120.5	0.24	41.4	0.087	2.90
CuZnCe-4	69.4	104.6	0.24	36.6	0.093	2.84
CuZnCe-5	36.8	53.7	0.32	19.2	0.170	2.74
CuZnCe-6	66.7	107.6	0.70	34.7	0.28	3.05
CuZnCe-7	48.4	78.4	0.17	25.5	0.087	2.94
CuZnCe-8	49.6	73.5	0.17	26.1	0.079	2.79

Reaction conditions: catalyst weight = 100 mg; reaction temperature = 230 °C; $H_2O/CH_3OH = 1.6$; liquid flow rate = 2.0 cm^3/h; $O_2/CH_3OH = 0.25$; flow rate of air = 8.8 cm^3/min. No carrier gas. Results collected after 12 h of on-stream operation.
[a]Outlet CO level determined using a methanizer-FID GC assembly.
[b]Ratio of rate of H_2 production to rate of methanol conversion.

as well as $Ce(III)NO_3$ salts as precursors. However, the catalysts obtained by using $Ce(IV)SO_4$ or $Ce(III)NO_3$ are less active in terms of both methanol conversion and H_2 production rate compared with the catalyst prepared using CAN salt for a given Ce content (compare the data of CuZnCe-3 with those of CuZnCe-6 and CuZnCe-7). The catalytic activity decreases to a large extent when $Ce(III)NO_3$ is used as a precursor.

4. Discussion

4.1. Effect of Zr substitution

The observed differences in the EPR patterns (figure 3) between the Al-containing samples (CuZnZr-1 and CuZnZr-2) and the Zr-containing sample (CuZnZr-3) leads to a conclusion that the presence of Al results in the formation, at the surface, of more isolated Cu^{2+} ions that interact with Al. These isolated Cu^{2+} ions, therefore, would be reduced at relatively higher temperatures, thus exhibiting a broad TPR profile (figure 2). In contrast, such isolated Cu^{2+} ions (those interacting with Al) are absent in CuZnZr-3 and the sample consists largely of clustered Cu^{2+} ions, which is easily reducible as evidenced from the TPR results.

The higher BE of CuZnZr-1 and CuZnZr-2 compared to that of CuZnZr-3 clearly indicates that the electron density on Cu^{2+} is less in the former samples, or, in other words, they are more electropositive compared to the CuZnZr-3 sample. The AES results (figure 5) corroborate the core-level XPS results by exhibiting a similar trend in the KE of Auger electrons as well as the modified Auger parameter α'. The KE of Auger electrons for CuZnZr-1 and CuZnZr-2 is around 916.9 eV, which is similar to that of malachite ($Cu(OH)_2CuCO_3$) or $CuAl_2O_4$ (see table 3) while for CuZnZr-3 it appears at 918.0 eV, close to that of CuO [20–22]. The formation of surface $CuAl_2O_4$ spinel is often noticed when Al is present in the sample [32]. In XPS, the $CuAl_2O_4$ surface spinel species are characterized by a higher $Cu2p_{3/2}$ BE (by ~ -1 eV) and a lower Auger KE of Cu LMM compared to that of CuO. Thus, the higher BE and lower Auger KE of CuZnZr-1 and CuZnZr-2 catalysts could be due to the formation of surface $CuAl_2O_4$ species, and this is in agreement with the results derived from EPR and TPR. The existence of a Cu–Al interaction in those Al-containing samples impedes the reducibility of Cu^{2+} and CuZnZr-3, without Al, exhibited the highest reducibility.

The Zr 3*d* XPS of Zr-containing catalysts (figure 6) clearly shows the existence of zirconium sites (species II) with relatively high electron density. The results reveal that some of the Zr dissolves in the CuO lattice to form a "Cu–O–Zr–O" solid solution. The existence of the "Cu–O–Zr" bond in the CuZnZr-3 catalyst has been clearly identified by extended X-ray absorption fine structure (EXAFS) analysis (results not shown) [33]. The formation of the "Cu–O–Zr" bond in the Zr-containing catalysts brings about a synergistic interaction between Cu and Zr and this could also facilitate the reduction of Cu^{2+} species.

The low BE of the main VB involving Cu 3*d* valence electrons in CuZnZr-3 and splitting of the Cu 3*d* anti-bonding levels from the main VB (figure 7) clearly indicates that the Cu 3*d* anti-bonding orbitals are significantly populated in these catalysts. The relatively high intensity of the shoulder at 2.3 eV corresponding to the Cu 3*d* anti-bonding orbitals in CuZnZr-3 supports the fact that the splitting of the main VB is more pronounced in this catalyst. This could also be responsible for the improved reducibility of Cu^{2+} in this sample as observed by TPR.

Based on the TPR, EPR and XPS results, the higher catalytic performance of the CuZnZr-3 catalyst can be attributed to the enhanced copper reducibility due to the operation of a synergistic interaction between copper and zirconium. The involvement of a Cu^{o}/Cu_{ox} redox mechanism in the methanol synthesis and methanol decomposition reactions is well known in the literature [2,34]. Hence, the ease of reducibility is likely to be an important factor in determining the efficiency of the catalysts in the reforming reaction as well. Furthermore, the CuZnZr-3 catalyst exhibits the highest copper surface area and copper metal dispersion and the smallest crystallite size (see table 2) thereby improving the synergy between CuZn and Zr. Similar results were also reported very recently in the steam reforming of methanol over Cu/Zn/Zr catalysts with Cu:Zn:Zr molar ratio = 70:18:12 [5,35].

4.2. Effect of Ce substitution

The data shown in table 6 indicate that the substitution of Ce in the CuZn-based catalysts shows no significant improvement in the catalytic performance although methanol conversion improved slightly over the catalyst containing around 20 wt% Ce. This study reveals that under the present experimental conditions used for the OSRM reaction, the Ce does not participate in the water-gas shift reaction or CO oxidation in the subsequent step. Further modifications of the catalyst preparation method, catalyst composition and reaction operating parameters are currently underway in order to produce H_2 suitable for fuel cells preferably in a single step.

5. Conclusions

Substitution of Zr for Al in the CuZnAl(Zr) oxide catalysts improved the catalytic performance because of an enhancement in copper reducibility and metal dispersion as a result of the formation of a "Cu^{2+}–O–Zr^{4+}–O–" solid solution at the surface of the catalyst. In

the catalysts containing Zr, the Cu 3*d* anti-bonding orbitals split from the main VB and shift towards lower BE and this also accounts for the improved redox properties of the Zr-containing catalyst. The presence of zirconium in these catalyst systems brings about a synergistic interaction with copper species.

Under the experimental conditions employed in the present study the substitution of Ce in the CuZn-based catalytic systems has no significant promotional effect on the catalytic performance in the OSRM reaction, although the methanol conversion and H_2 production rate are improved to some extent over catalyst containing around 20 wt% Ce.

Acknowledgments

The authors would like to express their sincere gratitude to Dr. M. Okazaki of our institute and Dr. C.S. Gopinath, National Chemical Laboratory, Pune, India, for the EPR and XPS measurements, respectively, and many fruitful discussion. Financial support from Aichi Science and Technology Foundation (ASTF) and also the Japan Science and Technology Corporation (JST) is gratefully acknowledged.

References

[1] W.-H. Cheng and H.H. Kung, *Methanol Production and Use* (Marcel Dekker, New York, 1994) p. 1.
[2] W.-H. Cheng, Acc. Chem. Res. 32 (1999) 685.
[3] Y. Matsumura, K. Kagawa, Y. Usami, M. Kawazoe, H. Sakurai and M. Haruta, Chem. Commun. (1997) 657.
[4] L. Alejo, R. Lago, M.A. Peña and J.L.G. Fierro, Appl. Catal. A: General 162 (1997) 281.
[5] J.P. Breen and J.R.H. Ross, Catal. Today 51 (1999) 521.
[6] Y. Matsumura, K. Tanaka, N. Tode, T. Yazawa and M. Haruta, J. Mol. Catal. A: Chemical 152 (2000) 157.
[7] Y. Liu, K. Suzuki, S. Hamakawa, T. Hayakawa, K. Murata, T. Ishii and M. Kumagai, Chem. Lett. (2000) 486.
[8] S. Velu, K. Suzuki and T. Osaki, Chem. Commun. (1999) 2341.
[9] S. Velu, K. Suzuki, M. Okazaki, M.P. Kapoor, T. Osaki and F. Ohashi, J. Catal. 194 (2000) 373.
[10] S. Velu, K. Suzuki and T. Osaki, Catal. Lett. 69 (2000) 43.
[11] S. Velu, K. Suzuki, M.P. Kapoor, F. Ohashi and T. Osaki, Appl. Catal. A: General 213 (2001) 47.
[12] I.A. Fisher and A.T. Bell, J. Catal. 184 (1999) 357.
[13] A. Martinez-Arias, R. Cataluña, J.C. Conesa and J. Soria, J. Phys. Chem. B 102 (1998) 809.
[14] S. Velu, K. Suzuki and T. Osaki, Catal. Lett. 62 (1999) 159.
[15] J.F. Scholten and A. van Montfoort, J. Catal. 1 (1962) 85.
[16] G. Centi, S. Perathoner, D. Bigleno and E. Giamello, J. Catal. 151 (1995) 75.
[17] W. Dow, Y. Wang and T. Huang, J. Catal. 160 (1996) 155.
[18] E. Giamello, B. Fubini and P. Lauro, Appl. Catal. 21 (1986) 133.
[19] H. Praliand, S. Mikhailenko, Z. Chajar and M. Primet, Appl. Catal. B: Environmental 16 (1998) 359.
[20] I. Grohmann, B. Peplinski and W. Unger, Surf. Interf. Anal. 19 (1992) 591.
[21] G. Moretti, G. Fierro, M.L. Jacono and P. Porta, Surf. Interf. Anal. 14 (1989) 325.
[22] P. Porta, M.C. Campa, G. Fierro, M.L. Jacono, G. Minelli, G. Moretti and L. Stoppa, J. Mater. Chem. 3 (1993) 505.
[23] S. Ardizzone and C.L. Bianchi, Surf. Interf. Anal. 30 (2000) 77.
[24] J.J. Yeh and I. Lindau, I. At. Data Nucl. Data Tables 32 (1985) 1.
[25] S.V. Didziulis, K.D. Butcher, S.L. Cohen and E.I. Solomon, J. Am. Chem. Soc. 111 (1989) 7110.
[26] J. Lin, P. Jones, J. Guckert and E.I. Solomon, J. Am. Chem. Soc. 113 (1991) 8312.
[27] A. Martinez-Arias, J. Soria , R. Cataluña, J.C. Conesa and V. Cortés Corberan, Stud. Surf. Sci. Catal. 116 (1998) 591.
[28] M. Fernandez-Garcia, A. Martinez-Arias, A. Iglesias-Juez, C. Belver, A.B. Hungria, J.C. Conesa and J. Soria, J. Catal. 194 (2000) 385.
[29] M. Daturi, E. Finocchio, C. Binet, J. Lavalley, F. Fally, V. Perrichon, H. Vidal, N. Hickey and J. Kaspar, J. Phys. Chem. B 104 (2000) 9186.
[30] L. Kundakovic and M. Flytzani-Stephanopoulos, J. Catal. 179 (1998) 203.
[31] A. Martinez-Arias, M. Fernandez-Garcia, O. Galrez, J.M. Coranado, J.A. Anderso, J.C. Conesa, J. Soria and G. Munuera, J. Catal. 195 (2000) 207.
[32] R.T. Figueiredo, A. Martinez-Arias, M.L. Granados and J.L.G. Fierro, J. Catal. 178 (1998) 146.
[33] S. Velu, K. Suzuki, C.S. Gopinath, H. Yoshida and T. Hattori, Phys. Chem. Chem. Phys. 4 (2002) 1990.
[34] G. Fierro, M.L. Jacono, M. Inversi, P. Prta, F. Cioci and R. Lavecchia, Appl. Catal. A: General 137 (1996) 327.
[35] J.P. Breen, F.C. Meunier and J.R.H. Ross, Chem. Commun. 2247 (1999).